Theoretical investigation on the mechanism and kinetics of OH radical with m-xylene

Mingqiang Huang [a,*], Zhenya Wang [b], Liqing Hao [b], Weijun Zhang [b]

[a] Department of Environmental Science and Engineering, Xiamen University, Tan Kah Kee College, Zhangzhou 363105, PR China
[b] Laboratory of Environment Spectroscopy, Anhui Institute Of Optics & Fine Mechanics, Chinese Academy Of Sciences, Hefei 230031, PR China

ARTICLE INFO

ABSTRACT

The OH hydrogen abstraction and addition with m-xylene have been studied in the range of 298–1000 K using quantum chemistry methods. The geometries and frequencies of the reactants, transition states and products have been performed at BHandHLYP/6-311++G(d,p) level, and single-point calculation for all the stationary points were carried out at CCSD(T) calculations of the optimized structures with the same basis set. Eight different reaction paths are considered, corresponding to side chain, three possible ring hydrogen abstraction and four kinds different OH addition. The results of the theoretical study indicate that the reaction proceeds almost exclusively through OH addition at room temperature, and is predicted to occur dominantly at the ortho position, and the calculated overall rate constant is 2.60×10^{-11} cm^3 molecule^{-1} s^{-1}, showing the agreement with available experimental data extremely. Despite unimportance at low temperature, at 1000 K ring hydrogen abstraction accounts for about 70% of the total abstraction reaction, and the whole hydrogen abstraction makes up for 3% of the total reaction. This study may provide useful information on understanding the mechanistic features of OH-initiated oxidation of m-xylene.

1. Introduction

The occurrence of high levels of monocyclic aromatic compounds in urban areas is linked to anthropogenic activity directly such as fossil burning and solvent use [1–3]. The aromatic hydrocarbons contribute to the problems of urban air pollution severely today. Besides their carcinogenic and mutagenic effects on living organisms and human health, in the presence of NO$_x$, the degradation of these compounds in the troposphere contributes substantially to the ozone and photooxidant burden and also the formation of secondary organic aerosol (SOA) [4–7], which are known to be harmful to human and ecosystem health [8–10]. As emissions of aromatic hydrocarbons are concentrated in urban areas, where many people live and work, the formation of SOA becomes a more acute problem [11].

In the atmosphere, the reaction of aromatic compound with OH radical corresponds to the major atmospheric loss process during daylight hours. The OH-initiated reaction of aromatic compound results in minor H-abstraction and major OH addition to the aromatic ring (about 90%) [12,13]. There has been considerable experimental and theoretical work on the OH-initiated reactions of aromatic compound. Experimental studies have investigated the

temperature and pressure dependent rate constant of the initial OH-aromatic reaction [14–19]. The room temperature rate constant for OH-aromatic reaction is on the order of 10^{12} cm^3 molecule^{-1} s^{-1}. The OH-aromatic reaction also has been studied using computational methods previously. Glauco Tonachini et al. [20,21], Joseph Bozzelli et al. [22], Tokmakov et al. [23], and Michael Pilling et al. [24] reported extensive theoretical investigations on the OH-benzene reaction. Bortolotti and Edney [25], Uc and co-workers [26], and Suh et al. [27,28] have performed quite similar investigations, looking at the initial attack of OH on toluene using density functional-based methods. Renyi Zhang et al. [29,30] and Huang et al. [31] have presented the investigation of the mechanistic features of OH-initiated oxidation reactions of xylene using consistent density function theory (DFT). In these theoretical works, the thermochemical properties of intermediates, OH adduct, prereaction complex, the structures and properties of the important transition states were obtained. As shown in Table 1, their transition state theory calculations succeeded in reproducing the observed experimental rate constant at room temperature. However, these theoretical calculations performed H-abstraction or OH addition separately. As for OH-xylene reactions, theoretical calculations on the formation of OH adduct isomers have been reported by Renyi Zhang et al. [28,29] and Huang et al. [30], no theoretical investigation including the H-abstraction channels which have been reported so far.

* Corresponding author. Tel.:+86 551 5593174; fax: +86 551 5591551.
E-mail address: huangmingqiang@gmail.com (M. Huang).

Table 1
Comparison between theoretical and experimental rate coefficient for OH-aromatic reaction at 298 K.

Reaction	Theoretical(overall) (cm^3 molecule^{-1} s^{-1})	Refs.	Experimental (cm^3 molecule^{-1} s^{-1})	Refs.
Benzene-OH	1.4×10^{-12}	[23]	$(1.59 \pm 0.12) \times 10^{-12}$	[14]
Toluene-OH addition	1.0×10^{-11}	[27]	$(6.40 \pm 0.24) \times 10^{-12}$	[15]
Toluene-OH H abstraction	2.40×10^{-13}	[26]	4.25×10^{-13}	[16]
p-Xylene-OH addition	9.24×10^{-12}	[29]	$(13.5 \pm 1.4) \times 10^{-12}$	[17]
m-Xylene-OH addition	2.60×10^{-11}	This work	$(23.4 \pm 0.7) \times 10^{-12}$	[19]

m-Xylene is an important constitution of aromatic hydrocarbons and high reactive with respect to ozone and secondary organic aerosol formation [12]. Photochemical oxidation of *m*-xylene is mainly initiated by attacking from hydroxyl radicals OH. The OH-*m*-xylene reaction results in hydrogen atom abstraction from the methyl group or aromatic ring and OH addition to the ring [13]. As shown in Fig. 1, the mechanistic complexity of the *m*-xylene oxidation arises from multiple isomeric pathways. Hydrogen atom abstraction results in M–H–S, M–H–O, M–H–P, and M–H–M, four possible isomers, and OH addition to *m*-xylene results in four distinct structural OH-*m*-xylene adduct isomers (i.e., MI, MO, MP, and MM). There are several products and kinetic studies on OH reaction with *m*-xylene [19,32,33]. The rate constant of *m*-xylene reported by Ohta at room temperature is $(23.4 \pm 0.7) \times 10^{-12}$ cm^3 molecule^{-1} s^{-1}, much higher than that of OH-toluene reaction [19]. In the experimental study of OH-initiated reactions of *m*-xylene using GC/MS detection, Forstner and co-workers [32] observed major products such as dimethylphenols, 4-oxo-2-pentenal, and 2-methyl-4-oxo-2-butenal. Currently, the explicit mechanism of *m*-xylene oxidation following the initial OH attacking remains highly uncertain. Therefore, in the present work, we present a comprehensive theoretical investigation of the reaction of OH with *m*-xylene, including hydrogen abstraction and OH addition. Reaction energies for the formation of the aromatic radicals have been obtained to determine their relative stability, and rate coefficients in the range 298–1000 K have been analyzed to assess the favorable pathways to propagate the *m*-xylene oxidation.
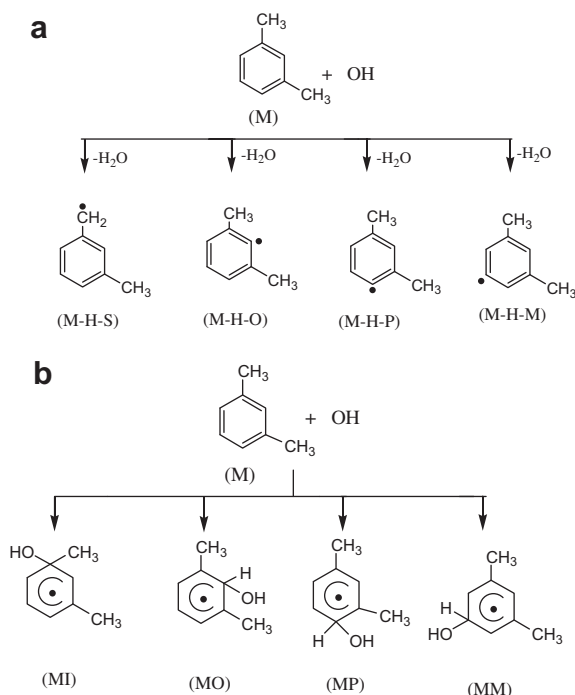

Fig. 1. (a) Suggested pathways of OH hydrogen abstraction with *m*-xylene. (b) Suggested pathways of addition of OH to *m*-xylene.

2. Computational methods

As pointed out by Uc et al. [26], the methodology of geometry optimization and frequency calculations at the BHandHLYP/6-311++G(d,p) followed by CCSD(T) calculation with the same basis set is found to yield excellent results for the OH reaction with toluene. Hence, geometry optimizations and frequency analyses are performed at the BHandHLYP/6-311++G(d,p) level of theory, and single-point calculations are performed at CCSD(T) calculation with the same basis set. The zero-point vibration energy (ZPVE) at the BHandHLYP/6-311++G(d,p) level is also included. To confirm the obtained transition states connected with the right reactants and products, the intrinsic reaction coordinate (IRC) calculations were performed at BHandHLYP/6-311++G(d,p) level. All computations were carried out by using the Gaussian98 program [34].

Rate coefficients were calculated to apply to the transition state theory (TST) as implementing in TheRate program 1.0 [35]. According to the transition state theory under the condition of gas reaction, the rate constant, $k(T)$, is expressed by[36].

$$k(T) = \frac{k_B T}{h} \frac{Q_{TS}}{Q_R} e^{-E_a/K_B T}$$

where the Q are the partition functions of the transition states and the reactants and k_B is Boltzmann's constant, and E_a is the net activation energies.

3. Result and discussion

3.1. Side chain hydrogen abstraction

The OH-*m*-xylene reaction can result in H-atom abstraction from the methyl group, leading to the formation of M–H–S. The optimized geometries of the M–H–S and its corresponding transition states are represented in Fig. 2, where we have indicated the main angles and distances. The side chain transition states turn out the similar ones obtained for OH abstraction of a primary hydrogen atom from alkanes and toluene [26,37] previously. In Table 2, geometrical parameters for the abstraction transition state in methane, ethane, for the primary hydrogen atoms in propane and toluene are also reported for comparison. Thus, these transition states are characterized by the following general properties: (1) It is closer from reactants than products. The distances of CH are smaller than those of O···H, meaning that it occurs at the beginning of the reaction, when the OH radical is still somewhat far apart. The results agree with the Hammond postulate, according to transition states of exothermic reactions which should be more reactant-like than product-like. However, for alkanes, the distance of O···H is about 1.27 Å, typically, in toluene it is 1.35 Å, and in *m*-xylene, it is 1.36 Å in TS_M–H–S, indicating that in *m*-xylene abstraction the OH radical is further from the hydrogen atom which is being abstracted. IRC analysis shown that TS_M–H–S is transition state early, the C···H distance being less than 0.11 Å from the normal C—H bond in the methyl group of *m*-xylene. (2) The distance of C···O in C···H···O is approximate equal to 2.5 Å, and the C···H···O angle is close to 170°. It is curved in a direction
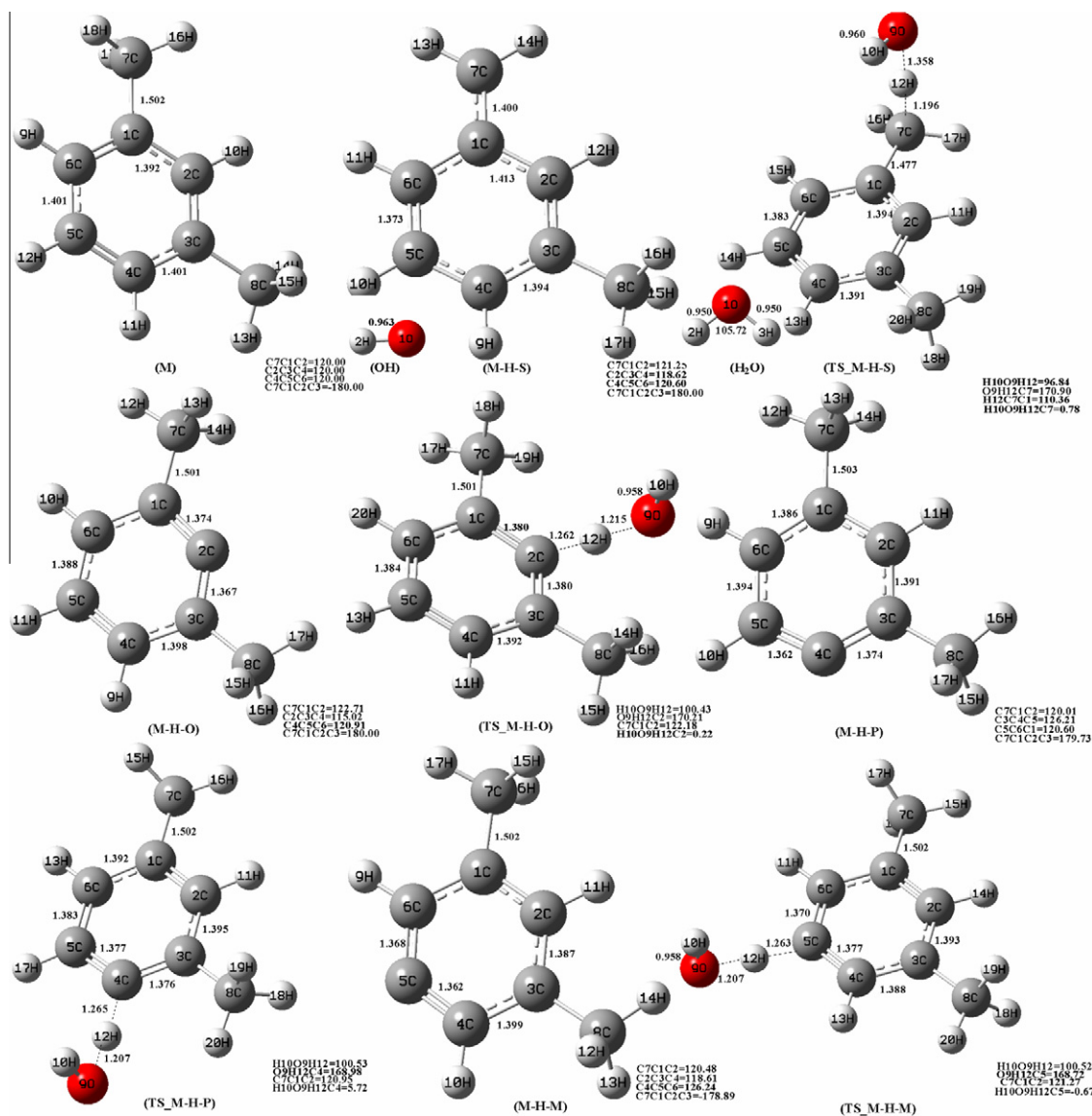
Fig. 2. Optimized geometries of hydrogen abstraction products and their corresponding transition states at the BHandHLYP/6-311++G(d,p) level of theory Bond length (Å) Bond angle(°).

Table 2
Comparison of main geometrical parameters (Bonds (Å), angles (°)) of TSs with corresponding values in primary hydrogen abstraction in small alkanes and toluene.

	O···H	O–H(bond)	C···H	O···H···C(α)
CH_4···OH	1.23	0.96	1.25	171.18
C_2H_6···OH	1.27	0.95	1.22	170.66
C_3H_8···OH_{prim}	1.27	0.95	1.23	170.15
Toluene···OH	1.35	0.96	1.20	175.0
TS_M–H–S	1.36	0.96	1.20	170.9

that is the H of the OH radical is in a cis position to the C atom. The transition vector for side chain H abstraction clearly shows the approach of the OH radical toward a hydrogen atom of the methyl group. At the CCSD(T)//BHandHLYP level, the activation energies (E_a) for M–H–S is 3.14 kcal mol^{-1}. Bravo-Pérez et al. [37] caculated the barrier height of 3.53, 2.05 and 2.54 kcal mol^{-1} for methane, ethane, and toluene hydrogen abstraction, respectively, only slightly higher than our calculations.

3.2. Ring hydrogen abstraction

The BHandHLYP method was employed to optimized the transition state geometries for abstraction of an ortho, meta, para hydrogen atom from the benzene ring. Structures are labeled TS_M–H–O, TS_M–H–P, TS_M–H–M, and they are shown in Fig. 2. In all of them, the oxygen atom of the OH radical lies in the plane of the ring, whereas the O—H bond is almost perpendicular to this plane. It can be seen that the distances of O···H and C···H are more symmetrical than the distances of TS_M–H–S, being about 1.21 and 1.26 Å, respectively. In fact, in these structures, the hydrogen atom has almost been transferred to oxygen by form of a water molecule. Thus, these transition states occur much later than in the case of the side chain hydrogen abstraction, and they have considerably larger barriers, as expected from the very small exothermicity of the reaction (about −0.40 kcal/mol at the CCSD(T) level). Relative energies of the transition states and products, calculated at the CCSD(T)//BHandHLYP level with the 6-311++G(d,p) basically sets are reported in Table 3. Imaginary frequencies of the transition states lie at about 1200 cm^{-1}, indicating tighter transition states

Table 3
ZPVE-corrected reaction energies (RE), activation energies (E_a), transition state's imaginary frequency, TST calculated rate constant k_{rec}, high-pressure limit unimolecular decomposition rate constant k_{uni}, branching ratios (R), and equilibrium constant K at 298 K.

Reaction	RE (kcal mol^{-1})	E_a (kcal mol^{-1})	k_{rec} (cm^3 molecule^{-1} s^{-1})	K_{uni} (s^{-1})	R	K
H-abstraction						
M + OH → M–H–S + H$_2$O	−24.21	3.14	1.56×10^{-13}	1.27×10^{-30}	0.0060	1.23×10^{16}
M + OH → M–H–O + H$_2$O	−0.41	8.80	6.77×10^{-15}	1.63×10^{-20}	0.00026	4.14×10^{5}
M + OH → M–H–P + H$_2$O	0.14	9.08	1.52×10^{-14}	5.64×10^{-20}	0.00059	2.70×10^{5}
M + OH → M–H–M + H$_2$O	−0.30	8.96	3.33×10^{-15}	3.72×10^{-19}	0.00013	8.96×10^{4}
OH-addition						
M + OH → MI	−12.43	5.14	4.89×10^{-13}	1.34×10^{4}	0.019	9.00×10^{4}
M + OH → MO	−13.55	2.80	1.57×10^{-11}	1.28×10^{3}	0.60	8.66×10^{5}
M + OH → MP	−13.04	3.60	7.32×10^{-12}	1.68×10^{3}	0.28	1.53×10^{6}
M + OH → MM	−11.74	5.57	2.28×10^{-12}	8.52×10^{4}	0.09	6.60×10^{4}

than in the case of side chain hydrogen abstraction. Reaction energies corrected for ZPE are reported in Table 3. The CCSD(T) energies barriers are 8.80, 9.08 and 8.96 kcal/mol for ortho, para, and meta position respectively. Ortho hydrogen abstraction yields the most stable product at the BHandHLYP level, however, differences are very small and all three products lie about 0.40 kcal/mol below reactants. No stabilizing interactions are observed in the transition states, which explains why the three transition states have very close energy values and also very similar imaginary frequencies.

3.3. OH addition

OH addition to *m*-xylene forms four possible isomers (Fig. 1(b)). Fig. 2 depicts the optimized geometries of the four adducts and their corresponding transition states obtained at the BHandHLYP/6-311++G(d,p) level of theory Fig. 3.

Addition of OH to *m*-xylene leads to a lengthening of C—C bonds adjunct to the site of addition. For the ipso isomer MI, the C—C bond lengths are increased by 0.106 Å between C1—C2 and C1—C6 and by 0.024 Å between C1 and C7 (the methyl carbon). The increased C—C bond length adjacent to the OH addition site reflects an increased σ character, as electron density is transferred to the newly formed C—O bonds. Similar C—C bonding characteristics are observed for MO, MP, and MM. For the isomer MO, the C—C bond lengths are increased by 0.111 Å between C1–C2 and by 0.118 Å between C2–C3. For the isomer MP, the C—C bond lengths are increased by 0.111 Å between C3–C4 and by 0.112 Å between C4–C5. And for the isomer MM, the C—C bond lengths are increased by 0.113 Å between C4–C5 and by 0.106 Å between C5–C6. The C—O bond distance is 1.434, 1.434, 1.432, and 1.428 Å for isomer MI, MO, MP, and MM, respectively. At the transition states, the C–O distance is 1.972 Å for MI, 1.971 Å for MO, 1.963 Å for MP, and 1.949 Å for MM. A comparison of the structures of *m*-xylene, the adduct isomers, and the transition states clearly reveals the intermediate features in the transition state structures.

Spin contamination with the BHandHLYP optimized geometries of the four adduct isomers is minimal. The calculated spin eigenvalues, $\langle S^{**}2 \rangle$, are 0.8417, 0.8427, 0.8391, and 0.8399 for MI, MO, MP, and MM, respectively. After the S + 1 component is annihilated, the values of $\langle S^{**}2 \rangle$ are reduced to 0.755 for four isomers, nearly identical to the exact value of a pure doublet. This implies that contamination of the unrestricted Hartree–Fock wave function from higher spin states is negligible for four isomers. ZPVE-corrected reaction energies and activation energies at the CCSD(T)//BHandHLYP level for the *m*-xylene-OH adduct formation are provided in Table 3. The reaction energies (RE) for MI, MO, MP, and MM are quite close, with the values of −12.43, −13.55, −13.04, and −11.74 kcal mol^{-1}, respectively. The activation energies (E_a) for MI, MO, MP, and MM are 5.14, 2.80, 3.60, and 5.57 kcal mol^{-1}, respectively. As the reaction energy for MO is higher than those

of MI, MP, and MM, suggesting MO is the most stable among these isomers.

The TST calculated rate constant of OH addition to *m*-xylene and the corresponding isomeric branching ratios at 298 K are listed in Table 3. Using BHandHLYP/6-311++G(d,p), we determined that the rate constant in the range 4.89×10^{-13}–1.57×10^{-11} cm^3 molecule^{-1} s^{-1}, with a total rate constant of 25.8×10^{-12} cm^3 molecule^{-1} s^{-1}, in agreement with the experimental value of $(23.4 \pm 0.7) \times 10^{-12}$ cm^3 molecule^{-1} s^{-1}[19]. The high-pressure limit unimolecular decomposition rate constant and equilibrium constant are also summarized in Table 3.

The decomposition rate constant of the four isomers of the OH-*m*-xylene adduct range from 1.28×10^{3} to 8.52×10^{4}. Our calculated equilibrium constants at 1 atm indicate that unimolecular decomposition of the OH-*m*-xylene adduct is too slow to compete with bimolecular recombination at room temperature. For the formation of MI, MO, MP, and MM, the branching ratios are 0.019, 0.60, 0.28, 0.09, respectively, suggesting a strong preference for the ortho addition of OH to *m*-xylene.

3.4. Kinetics

On the basis of the calculated activation energies and the transition state theory (TST), the rate constants for the hydrogen abstraction and OH addition are calculated. Eight rate constant coefficient were determined using TheRate program 1.0 [35], in the 298–1000 K temperature range. Results are listed in Table 3–5, and hydrogen abstraction (M–H), OH addition (M–OH), and the overall rate constants are also given. The branching ratios Γ_1 for ring abstractions with respect to the hydrogen abstraction, Γ_2 for hydrogen abstractions with respect to the overall reaction are given in Tables 4 and 5 as a function of temperature:

$$\Gamma_1 = \frac{k_{ring}}{k_{EB-H}} \times 100\%; \quad \Gamma_2 = \frac{k_{EB-H}}{k_{overall}} \times 100\%.$$

The TST calculated rate constant of OH addition to *m*-xylene and the corresponding isomeric branching ratios at 298 K are listed in Table 3. Using BHandHLYP/6-311++G(d,p) we determined that the rate constant in the range 4.89×10^{-13}–1.57×10^{-11} cm^3 molecule^{-1} s^{-1}, with a total rate constant of 2.58×10^{-11} cm^3 molecule^{-1} s^{-1}. The unimolecular decomposition rate constant and equilibrium constant are also summarized in Table 3. The decomposition rate constant of the for isomers of the OH-*m*-xylene adduct range from 1.28×10^{3} to 8.52×10^{4}.

Our calculated equilibrium constants at 1 atm indicate that unimolecular decomposition of the OH-*m*-xylene adduct is too slow to compete with bimolecular recombination at room temperature. For the formation of MI, MO, MP, and MM, the branching ratios are 0.019, 0.60, 0.28, 0.09, respectively, suggesting a strong preference for the ortho addition of OH to *m*-xylene. The subsequent
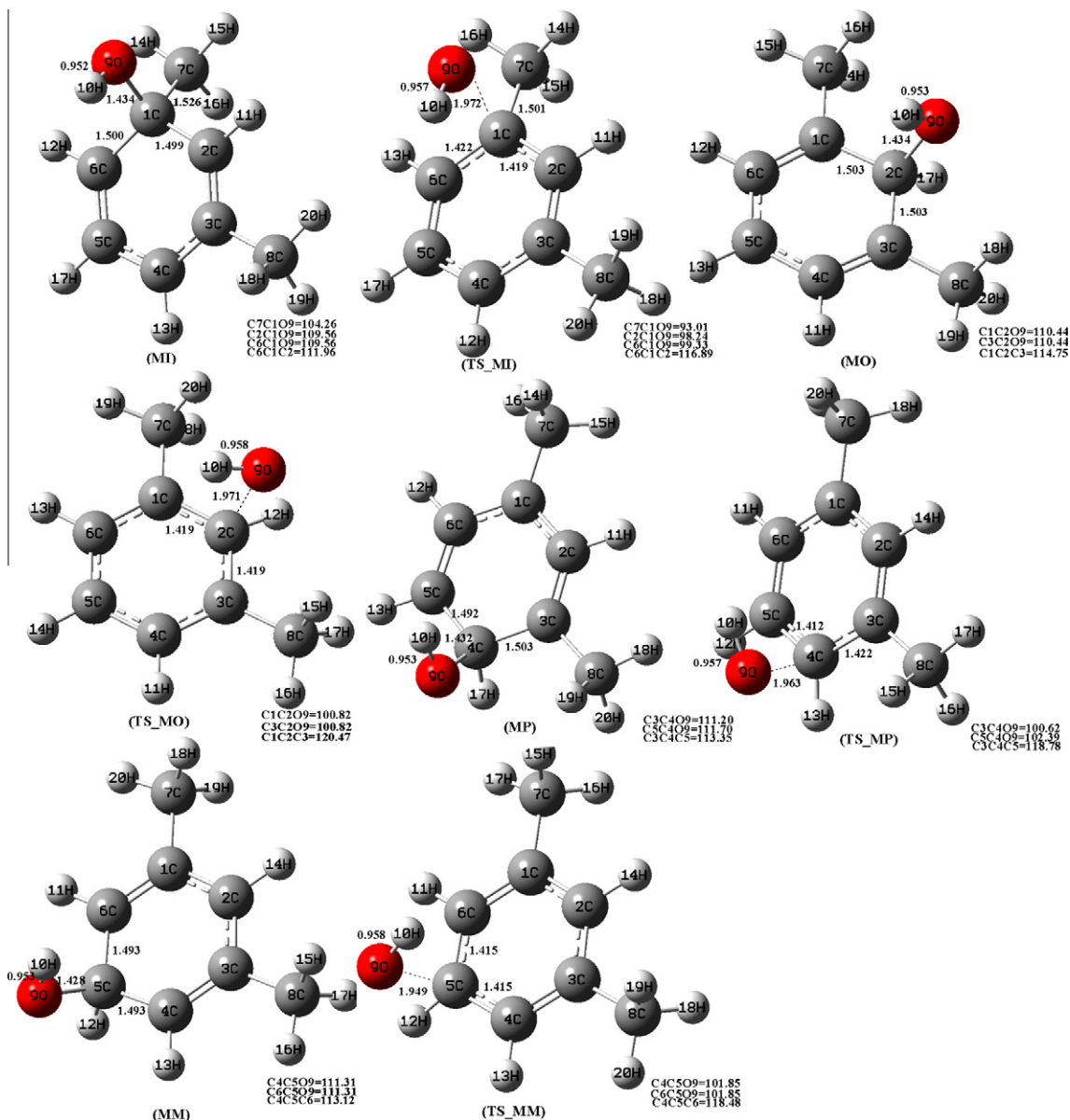
Fig. 3. Optimized geometries of ethylbenzene-OH adducts and their corresponding transition states at the BHandHLYP/6-311++G(d,p) level of theory bond length (Å) Bond angle(°).

Table 4
Partial and overall rate coefficients (cm^3 molecule^{-1} s^{-1}), tunneling corrections and branching ratio, $\Gamma_1 = k_{\text{ring}}/k_{\text{EB–H}} \times 100\%$ as a function of temperature of hydrogen abstraction reaction system.

T(K)	M–H–S	κ	M–H–O	κ	M–H–P	κ	M–H–M	κ	M–H	Γ_1 (%)
298	1.56×10^{-13}	0.005	6.77×10^{-15}	9.53	1.52×10^{-14}	10.26	3.33×10^{-15}	10.63	1.81×10^{-13}	13.98
400	1.98×10^{-13}	0.019	1.36×10^{-14}	4.64	3.45×10^{-14}	4.86	7.32×10^{-14}	4.96	3.19×10^{-13}	38.03
500	2.59×10^{-13}	0.042	2.47×10^{-14}	3.15	6.78×10^{-14}	3.25	1.42×10^{-13}	3.29	4.94×10^{-13}	47.46
600	3.39×10^{-13}	0.071	4.13×10^{-14}	2.48	1.20×10^{-13}	2.55	2.49×10^{-13}	2.57	7.49×10^{-13}	54.78
700	4.42×10^{-13}	0.10	6.49×10^{-14}	2.12	1.96×10^{-13}	2.16	4.05×10^{-13}	2.18	1.11×10^{-12}	59.99
800	5.70×10^{-13}	0.14	9.69×10^{-14}	1.89	3.01×10^{-13}	1.93	6.22×10^{-13}	1.93	1.59×10^{-12}	64.14
900	7.25×10^{-13}	0.17	1.39×10^{-13}	1.74	4.41×10^{-13}	1.77	9.11×10^{-13}	1.77	2.22×10^{-12}	67.16
1000	9.10×10^{-13}	0.21	1.92×10^{-13}	1.63	6.22×10^{-13}	1.65	1.28×10^{-12}	1.66	3.00×10^{-12}	69.80

reactions of MO leading to the formation of 2,4-dimethylphenol, which has observed in the *m*-xylene smog chamber experiments [32,33]. And for hydrogen abstraction, the rate constant of the five H-abstraction range from 3.33×10^{-15} to 1.56×10^{-13}, with a total

rate constant of 1.81×10^{-13} cm^3 molecule^{-1} s^{-1}, only account for 1% of the overall rate constant. We determined that the branching ratios of 0.006, 0.0003, 0.0006, and 0.0001 for the formation of M–H–S, M–H–O, M–H–P, and M–H–M, respectively, indicating a

Table 5
Partial and overall rate coefficients (cm^3 molecule^{-1} s^{-1}), tunneling corrections and branching ratio, $\Gamma_2 = k_{EB-H}/k_{overall} \times 100\%$ as a function of temperature of OH addition reaction system.

T(K)	MI	κ	MO	κ	MP	κ	MM	κ	M–OH	Overall	Γ_2 (%)
298	4.89×10^{-13}	0.61	1.57×10^{-11}	0.89	7.32×10^{-12}	0.39	2.28×10^{-12}	0.24	2.58×10^{-11}	2.60×10^{-11}	0.70
400	5.44×10^{-13}	2.20	1.73×10^{-11}	2.16	8.51×10^{-12}	2.09	2.80×10^{-12}	0.61	2.92×10^{-11}	2.95×10^{-11}	1.08
500	6.45×10^{-13}	4.74	2.03×10^{-11}	7.40	1.03×10^{-11}	5.66	3.51×10^{-12}	1.07	3.48×10^{-11}	3.52×10^{-11}	1.40
600	7.81×10^{-13}	7.89	2.43×10^{-11}	16.81	1.26×10^{-11}	10.99	4.40×10^{-12}	7.80	4.21×10^{-11}	4.28×10^{-11}	1.75
700	9.49×10^{-13}	11.35	2.92×10^{-11}	30.18	1.54×10^{-11}	17.65	5.48×10^{-12}	10.18	5.10×10^{-11}	5.21×10^{-11}	2.13
800	1.15×10^{-12}	14.91	3.49×10^{-11}	46.80	1.86×10^{-11}	25.17	6.74×10^{-12}	12.42	6.14×10^{-11}	6.30×10^{-11}	2.52
900	1.38×10^{-12}	18.43	4.13×10^{-11}	65.81	2.23×10^{-11}	33.18	8.19×10^{-12}	14.51	7.32×10^{-11}	7.54×10^{-11}	2.94
1000	1.64×10^{-12}	21.83	4.89×10^{-11}	86.44	2.65×10^{-11}	41.37	9.84×10^{-12}	16.42	8.69×10^{-11}	8.99×10^{-11}	3.34

strong preference for the methyl H-abstraction. The ring abstraction accounts for only 14% of the total abstraction reaction, it can be negligible at the atmospheric conditions. The predicted overall rate constant for OH with *m*-xylene is 26.0×10^{-12} cm^3 molecule^{-1} s^{-1}. This value is showing a very good agreement with the experimental value of $(23.4 \pm 0.7) \times 10^{-12}$ cm^3 molecule^{-1} s^{-1}[19].

As can be observed in Tables 4 and 5, at low temperature the hydrogen abstraction proceeds almost exclusively through side abstraction, however, at 1000 K ring hydrogen abstraction accounts for about 70% of the total abstraction reaction. These results confirm the proposal of Tully et al. that, at high temperatures, abstraction of ring hydrogen atoms becomes nonnegligible [38]. However, even at 1000 K, the whole hydrogen abstraction makes up only for 3% of the total reaction. Our results indicate a smaller contribution from ring hydrogen abstraction channels than estimated by Tully et al. from a simple comparison between the overall OH abstraction reaction rate constants in benzene and toluene. Although these authors suggest a 20% ring abstraction at 500 K, calculations predict that this branching ratio occurs well above 1000 K.

4. Conclusion

The present theoretical results provide several new insights into the mechanism of OH-initiated oxidation of *m*-xylene. The energies and rate constant of the eight possible channels have been estimated on the basis of the quantum chemical calculations, and the dominant channels at the room temperature were confirmed to be the OH addition to the ortho position, and the calculated overall rate constant is 2.60×10^{-11} cm^3 molecule^{-1} s^{-1}, showing a very good agreement with available experimental data. However, at the high temperature, hydrogen abstraction and abstraction of ring hydrogen atoms becomes nonnegligible. At 1000 K, ring abstraction accounts for about 70% of the total abstraction reaction, and the whole hydrogen abstraction makes up for 3% of the total reaction.

Acknowledgements

Reference

[1] M.A. Dearth, C.A. Glerczak, W.O. Slegl, Environ. Sci. Technol. 26 (1992) 1573.
[2] T. Tanaka, T. Samukawa, Chemosphere 33 (1996) 131.
[3] T. Etzkorn, B. Klotz, S. SØrensen, I.V. Partroescu, I. Barnes, K.H. Becker, U. Platt. Atmos. Environ. 33 (1999) 525.
[4] J.F. Pankow, Atmos. Environ. 28 (1994) 188.
[5] J.R. Odum, T.P.W. Jungkamp, R.J. Griffin, R.C. Flagan, J.H. Seinfeld, Science 276 (1997) 96.
[6] J. Yu, H.E. Jeffries, K.G. Sexton, Atmos. Environ. 31 (1997) 2261.
[7] M.S. Jang, R.M. Kamens, Environ. Sci. Technol. 35 (2001) 3626.
[8] C. Pilinis, S.N. Pandis, J.H. Seinfeld, J. Geophys. Res. 100 (1995) 18739.
[9] E. Annmarie, M.L. Susan, R.H. Jeffrey, J.H. Kevin, R.C. Glen, Environ. Sci. Technol. 27 (1993) 626.
[10] J. Schwartz, D.W. Dockery, L.M. Neas, J. Air Waste Manage. Assoc. 46 (1996) 927.
[11] V. Cocheo, P. Sacco, C. Boaretto, E.D. Saeger, P.P. Ballesta, H. Skov, E. Goelen, N. Gonzalez, A.B. Caracena, Nature 404 (2000) 141.
[12] R. Atkinson, Atmos. Environ. 34 (2000) 2063.
[13] R. Atkinson, J. Arey, Chem. Rev. 103 (2003) 4605.
[14] D.D. Davis, W. Bollinger, S. Fisher, J. Phys. Chem. 79 (1975) 273.
[15] R.A. Perry, R. Atkinson, J.N. Pitts Jr., J. Phys. Chem. 81 (1977) 296.
[16] R. Kinspel, R. Koch, M. Siese, C. Zetzsch, Ber Bunsen-Ges. Phys. Chem. 94 (1990) 1375.
[17] J.M. Nicovich, R.L. Thompson, R.L. Thompson, A.R. Ravishankara, J. Phys. Chem. 85 (1981) 2913.
[18] R. Atkinson, S.M. Aschmann, J. Int. Chem. Kinet. 23 (1991) 77.
[19] T. Ohta, T. Ohyama, Bull. Chem. Soc. Jpn. 58 (1985) 3029.
[20] G. Ghigo, G. Tonachini, J. Am. Chem. Soc. 120 (1998) 6753.
[21] F. Motta, G. Ghigo, G. Tonachini, J. Phys. Chem. A. 106 (2002) 4411.
[22] C.C. Chen, J.W. Bozzelli, J.T. Farrell, J. Phys. Chem. A. 108 (2004) 4632.
[23] I.V. Tokmakov, M.C. Lin, J. Phys. Chem. A. 106 (2002) 11309.
[24] D.R. Glowacki, L.M. Wang, M.J. Pilling, J. Phys. Chem. A 113 (2009) 5385.
[25] L.J. Bortolotti, E.O. Edney, Chem. Phys. Lett. 245 (1995) 119.
[26] V.H. Uc, J.R. Alvarez-Idaboy, A. Galano, I. Garcia-Cruz, A. Vivier-Bunge, J. Phys. Chem. A. 110 (2006) 10155.
[27] I. Suh, D. Zhang, R. Zhang, L.T. Molina, M.J. Molina, Chem. Phys. Lett. 364 (2002) 454.
[28] I. Suh, D. Zhang, R. Zhang, L.T. Molina, M.J. Molina, J. Am. Chem. Soc. 125 (2003) 12655.
[29] J. Fan, R. Zhang, J. Phys. Chem. A. 110 (2006) 7728.
[30] J. Fan, R. Zhang, J. Phys. Chem. A. 112 (2006) 4314.
[31] M. Huang, W. Zhang, Z. Wang, L. Hao, W. Zhao, X. Liu, B. Long, L. Fang, Int. J. Quant. Chem. 108 (2008) 954.
[32] H.J.L. Forstner, R.C. Flagan, J.H. Seinfeld, Environ. Sci. Technol. 31 (1997) 1345.
[33] J. Zhao, R. Zhang, K. Misawa, K. Shibuya, J. Photochem. Photobiol. A 176 (2005) 199.
[34] M.J. Frisch, G.W. Trucks, H.B. Schlegel, G.E. Scuseria, M.A. Robb, J.R. Cheeseman, V.G. Zakrzewski, J.A. Montgomery Jr., R.E. Stratmann, J.C. Burant, S. Dapprich, J.M. Millam, A.D. Daniels, K.N. Kudin, M.C. Strain, O. Farkas, J. Tomasi, V. Barone, M. Cossi, R. Cammi, B. Mennucci, C. Pomelli, C. Adamo, S. Clifford, J. Ochterski, G.A. Petersson, P.Y. Ayala, Q. Cui, K. Morokuma, D.K. Malick, A.D. Rabuck, K. Raghavachari, J.B. Foresman, J. Cioslowski, J.V. Ortiz, A.G. Baboul, B.B. Stefanov, G. Liu, A. Liashenko, P. Piskorz, I. Komaromo, R. Gomperts, R.L. Martin, D.J. Fox, T. Keith, M.A. Allaham, C.Y. Peng, A. Nanayakkara, C. Gonzalez, M. Challacombe, P.M.W. Gill, B. Johnson, W. Chen, M.M. Wong, J.L. Andres, C. Gonzalez, M. Head-Gordon, E.S. Replogle, J.A. Pople, Gaussian 98, Revision A. 7, Gaussian, Inc., Pittsburgh, PA, 1998.
[35] S. Zhang, T.N. Truong. VKLab version 1.0, University of Utah, 2001.
[36] C. Eckart, Phys. Rev. 35 (1930) 1303.
[37] G. Bravo-Pérez, J.R. Alvarez-Idaboy, J.A. Galano, A. Cruz-Torres, Chem. Phys. 310 (2005) 213.
[38] F.P. Tully, A.R. Ravishankara, R.L. Thompson, J.M. Nicovish, R.C. Shah, N.M. Kreutter, P.H. Wine, J. Phys. Chem. 81 (1981) 2262.